Photocatalytic CO_2 reduction over mesoporous TiO_2 photocatalysts

Reli Martin,[1] Nadrah Peter,[2] Filip Edelmannová Miroslava,[1] Ricka Rudolf,[1] Sever Škapin Andrijana,[2, 3] Lavrenčič Štangar Urška,[4] Kočí Kamila[1,*]

(1) Institute of Environmental Technology, CEET, VŠB-Technical University of Ostrava, 17. listopadu 15/2172, Ostrava-Poruba, 708 00, Czech Republic.

(2) Slovenian National Building and Civil Engineering Institute, Dimičeva ulica 12, 1000 Ljubljana, Slovenia.

(3) Faculty of Polymer Technology - FTPO, Ozare 19, 2380 Slovenj Gradec, Slovenia

(4) University of Ljubljana, Faculty of Chemistry and Chemical Technology, Večna pot 113, 1000 Ljubljana, Slovenia.

[*]E-mail: kamila.koci@vsb.cz, Phone: +420 596 997 354

Abstract

In this study, we investigated different synthesis methods (template-free and template-based) using copolymers of poly(ethylene oxide) and poly(propylene oxide) to enhance the CO_2 reduction activity of mesoporous TiO_2. Our main goal was to identify key factors affecting photocatalyst efficiency and selectivity. We compared the newly synthesized TiO_2 photocatalysts with the commercial photocatalyst P25. Among the materials studied, TiO_2-P123 in its pure anatase form demonstrated the highest photoreduction efficiency and CO_2 selectivity. In contrast, TiO_2-EG, TiO_2-F127, and P25, which contained both rutile and anatase phases, exhibited decreased photoactivity due to the formation of a type II heterojunction between the phases and higher oxygen adsorption on rutile's surface. Additionally, we observed that the choice of chemicals for photocatalyst preparation significantly influenced the specific surface area. TiO_2-P123, the most active photocatalyst, had the highest specific surface area, providing more reactive sites for improved light absorption efficiency and prolonged electron-hole pair lifetimes, resulting in enhanced photocatalytic activity. We also calculated apparent quantum yields to support our findings.

Keywords:

CO_2 reduction, TiO_2, photocatalysis, mesoporous material, sol-gel method

1. Introduction

The escalating levels of carbon dioxide (CO_2) emissions resulting from human activities, especially fossil fuels combustion, have triggered a rapid increase in global warming leading to climate change and the often overlooked acidification of the oceans [1]. Addressing the reduction of CO_2 levels released into the atmosphere has therefore become an urgent environmental topic demanding immediate attention. The development of effective strategies for mitigating CO_2 emissions has gained significant importance and priority. Many countries have implemented various plans of CO_2 emissions regulations, such as emissions trading systems or carbon taxation [2]. However, these regulations impose a great stress on companies as the European Union carbon permit price has increased more than fourfold in last 3 years. The majority of the developed world is trying to decarbonize the industry in the next few decades. However, it is important to mention that CO_2 is the most abundant source of carbon, which is not utilized. The photocatalytic reduction of CO_2 can harness the unlimited and free power in the form of sunlight and convert CO_2 into valuable chemicals and fuels using photocatalysts. This reaction holds immense promise as a sustainable solution to combat the climate change [3].

Photocatalytic reduction of CO_2, often called artificial photosynthesis, employs reducing agent, such as H_2O or H_2, and involves a series of intricate steps, including the adsorption of the CO_2 molecule on the photocatalyst surface, activation of CO_2 through photogenerated electron-hole pairs, and subsequent reduction of CO_2 to yield valuable products such as methane, methanol, and other hydrocarbons which desorb from the photocatalyst surface [3]. Since the goal is to use sunlight as the driving energy, this process is environmentally friendly and can be considered a renewable source of energy.

The photocatalytic reduction has been studied for decades, and over the past few years, substantial advancements have been made in the field of photocatalysts. Nevertheless, despite the progress made, numerous challenges need to be solved before the practical use of this revolutionary technology can be realized. This intricate, multi-electron process unfolds through a series of intricate steps, ultimately converting CO_2 molecules into valuable compounds like methane or methanol [4].

The key is to find a suitable photocatalyst. Without a doubt, the most studied photocatalyst is TiO_2, not only because of its excellent photocatalytic activity but also due to its low cost, chemical stability, and non-toxicity. The majority of published works have focused on improving TiO_2 photocatalytic activity through metal or non-metal doping, the formation of heterojunctions, or the deposition of precious metal [3, 5-7]. However, changing the pore

structure of TiO_2 can also affect its photocatalytic activity [8-11]. Each of these methods has its benefits, however, all of them increase the complexity and cost of the photocatalyst preparation [12-14].

This work focuses on the comparison of mesoporous TiO_2 synthesized via different sol-gel procedures reported in the literature, including both template-based and template-free routes. Templates, known as structure-directing agents (SDA), are molecules that form micelles under specific conditions. During the sol-gel procedures, the precursor (i.e. titanium alkoxide) is hydrolyzed and condensed into TiO_2 around the micelles, forming an ordered mesoporous structure after SDA removal. An alternative, template-free route begins with the reaction of titanium alkoxide with ethylene glycol, followed by hydrolysis at reflux temperature in water [15].

Herein, we report on the influence of the mesoporous TiO_2 synthesis procedure (template-free route and template-based route with two different copolymers of poly(ethylene oxide) and poly(propylene oxide)) on their CO_2 reduction activity. The employed sol-gel procedures use the same source of titanium ($Ti(Bu)_4$) but differ in other reactants and synthesis parameters that influence the properties of the synthesized TiO_2 and, consequently, the photocatalytic activity.

Even though each of the various chemicals used for the preparation was described in the literature before, to the best of our knowledge, they have never been compared within one study linking these synthesis procedures with photocatalytic activity in CO_2 reduction. Since comparison of photocatalyst efficiencies across studies is not possible because each group uses different experimental setups (e.g., photoreactor geometry, radiation source) and operating conditions (e.g., reducing agent, CO_2 concentration), the commonly used and commercially available TiO_2 P25 was used for comparison. In this work, it was found that the photocatalyst preparation used is of great importance, as it affects the phase composition and specific surface area of mesoporous TiO_2, which, in turn, influences the photocatalytic activity and selectivity during the photocatalytic reduction of CO_2.

Experimental details

1.1. Preparation of photocatalysts

Sample TiO_2-EG was synthesized according to Zhang et al. [16] using titanium n-butoxide (2 mL), which was mixed with ethylene glycol (50 mL) and stirred for 4 hours in nitrogen atmosphere. The reaction mixture was poured into a mixture of acetone (170 mL) and water (2.7 mL). The solid was collected and washed with ethanol by centrifugation. The

sample was then dried at 60 °C overnight and subsequently refluxed in water (100 mL) for 24 hours. The precipitate was collected and washed again with ethanol by centrifugation, followed by drying at 60 °C overnight. Finally, the solid was calcined at 650 °C for 2 hours with 5 °C/h ramp to yield 0.378 g of product.

Sample TiO_2-F127 was synthesized following the method described in Ma et al. [17]. Pluronic F127 (2.25 g) was dissolved in tetrahydrofuran (45 mL) with stirring, followed by the addition of 36% hydrochloric acid (6.9 mL) and acetic acid (2.9 mL). Titanium n-butoxide (5.1 mL) was slowly added to the solution during stirring. The reaction mixture was stirred for 15 minutes and then transferred into a volumetric flask, and heated at 40 °C for 20 hours and further heated at 80 °C for 8 hours without stirring. The solid was collected, washed with ethanol by centrifugation, and dried at 60 °C. Finally, the solid was calcined at 400 °C for 3 hours with 5 °C/h ramp to yield 0.671 g of product.

Sample TiO_2-P123 was synthesized following the method described in Chen et al. [18]. Pluronic P123 (1.74 g) was dissolved in ethanol (30 mL) with stirring at 40 °C. Titanium n-butoxide (10 mL) was dissolved in a mixture of ethanol (10 mL) and acetic acid (5 mL). This solution was then slowly added to the Pluronic P123 solution during stirring, followed by the addition of water (4 mL). The mixture was stirred for 2 hours and then left to stand at room temperature overnight. The solid was collected, washed with ethanol by centrifugation, dried at 60 °C, and then calcined at 400 °C for 4 hours with 2 °C/h ramp.

1.2. Characterization methods

A detailed description of the experimental apparatus and the characterization techniques used, namely X-ray powder diffraction (XRD), nitrogen adsorption method, UV-Vis spectroscopy, X-ray photoelectron spectroscopy (XPS) field emission scanning electron microscopy (FE-SEM), and photoelectrochemical measurements is provided in the Supplementary materials (Section S1.1).

1.3. Photocatalytic reduction of CO_2

Photocatalytic tests were performed in a batch mixed photoreactor (stainless steel, volume 357 ml, Fig.S1). The reaction mixture contained 100 ml of 0.2M NaOH with absorbed CO_2, and the investigated photocatalyst (0.1 g), was saturated by helium to purge the air. The reaction suspension was investigated for the photocatalytic reduction of CO_2 at pH 12 (saturated by helium). Based on our previous work, the amount of CO_2 absorbed from air is

more than enough, and an excess of CO_2 is not necessary [4]. An 8W Hg UVC lamp (peak intensity at 254 nm wavelength; Ultra-Violet Products Inc.; Fig.1) was used as the irradiation source and was placed on top of a quartz glass window incorporated into the photoreactor lid in a horizontal position. The reactor was sealed, and before the start of the reaction (switching on the lamp), a gaseous sample was taken (at time 0 h) through septum using a gas tight syringe. The gaseous samples were analyzed by a gas chromatograph (Shimadzu Tracera GC-2010Plus) equipped with BID (barrier discharge ionization detector). The reaction mixture was irradiated for 8 h. Gas samples were taken at 2, 4, 6, and 8 h for analysis. All measurements were performed reproducibly. Three products were detected from the photocatalytic reduction of CO_2: hydrogen, methane, and carbon monoxide. The photostability of photocatalysts is a very important to improve their practical use, and for all samples examined, photostability was confirmed by repeated measurements with the same batch resulting in reproducible yields of CO_2 photocatalytic reduction products [19-21].

2. Results and discussion

2.1. Characterization

Three samples were synthesized using different sol-gel procedures followed by calcination. The major crystal phase in all of the samples is anatase with minor inclusions of rutile and brookite in sample TiO_2-EG and rutile in sample TiO_2-F127. Specifically, sample TiO_2-EG contains 92 wt.% of anatase, 1.5 wt.% of rutile, and 6.5 wt.% of brookite, while TiO_2-F127 comprises only anatase and rutile, 83.5 wt.% and 16.5 wt.%, respectively. Sample TiO_2-P123 is composed solely of the anatase phase.

The crystal domain size of the anatase phase is approximately 20 nm in sample TiO_2-EG, about 13 nm in sample TiO_2-F127, and about 18 nm in sample TiO_2-P123, as determined using the Scherrer method. This method considers the full width at half maximum (FWHM) of the major reflection of the crystal phase. For anatase in these samples, the reflections were positioned at 25.30° 2θ (Fig. 1). The taken shape factor was 0.89, as anatase particles of that size resemble spheres [22]. The crystal domain sizes were not calculated for the rutile and brookite phases due to their low amounts, which would yield unreliable results. In the case of brookite, the major reflection overlaps with the anatase reflection at 25.30° 2θ. Nevertheless, it can be inferred that the brookite content is small since the reflection at 30.64° 2θ accounts for approximately 97 % of the full reflection at 25.33° 2θ (the structure was taken from [23]). Brookite and rutile crystallites tend to be larger due of their thermodynamic stability at sizes

above 11 nm (brookite) and 35 nm (rutile). They become thermodynamically more stable at larger sizes because they have higher surface energy than anatase but lower bulk energy than anatase. As a consequence, rutile, and to some extent brookite, become the most favorable crystal phases as their size exceeds the mentioned thresholds [24]. However, it is important to note that actual particle sizes may differ from these thermodynamic calculations due to the kinetics of transformation between the polymorphs.

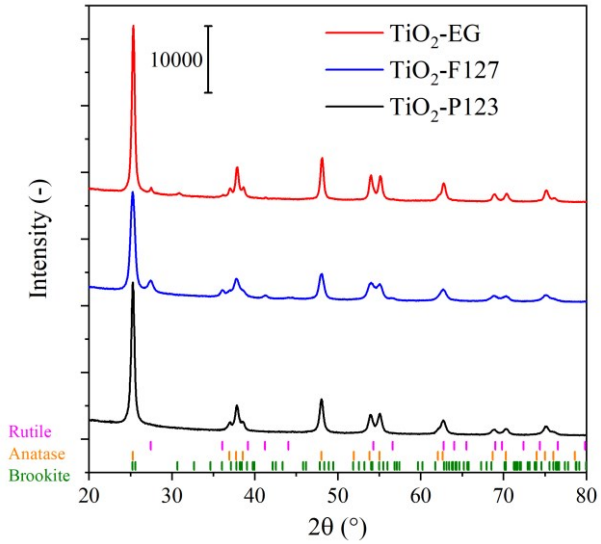

Figure 1: X-ray diffraction patterns of investigated photocatalysts.

All three materials exhibit a type IV isotherm according to IUPAC [25]. For TiO_2-EG, the hysteresis loop of H1 type is positioned at the highest relative pressure (Fig. 2a). This material has a relatively narrow distribution of pore volume by pore diameter. According to the literature [16], the hydrolysis step is crucial for obtaining a porous structure. TiO_2-F127 has relatively broad hysteresis loop, which could result from both mesoporous intraparticle porosity (0.5-0.8 p/p^0) and interparticle porosity (0.8-1.0 p/p^0). The loop exhibits features of H3 type in the lower p/p^0 region. The presence of the first hysteresis is expected due to the use of SDA during synthesis. TiO_2-P123 exhibits H2(a) type of hysteresis loop with significant pore blocking, which is commonly caused by ink bottle shaped pores. TiO_2-EG and TiO_2-F127 have smaller BET specific surface areas (48 and 58 m^2/g, respectively), while TiO_2-P123 has significantly higher value at 82 m^2/g. The pore volumes (up to 0.9 p/p^0 ~ 21 nm) of TiO_2-EG, TiO_2-F127, and TiO_2-P123 are 0.13,0.12, and 0.11 cm^3/g, respectively (Fig. 2b). The information obtained from XRD and N_2 physisorption techniques is summarized in Table 1.

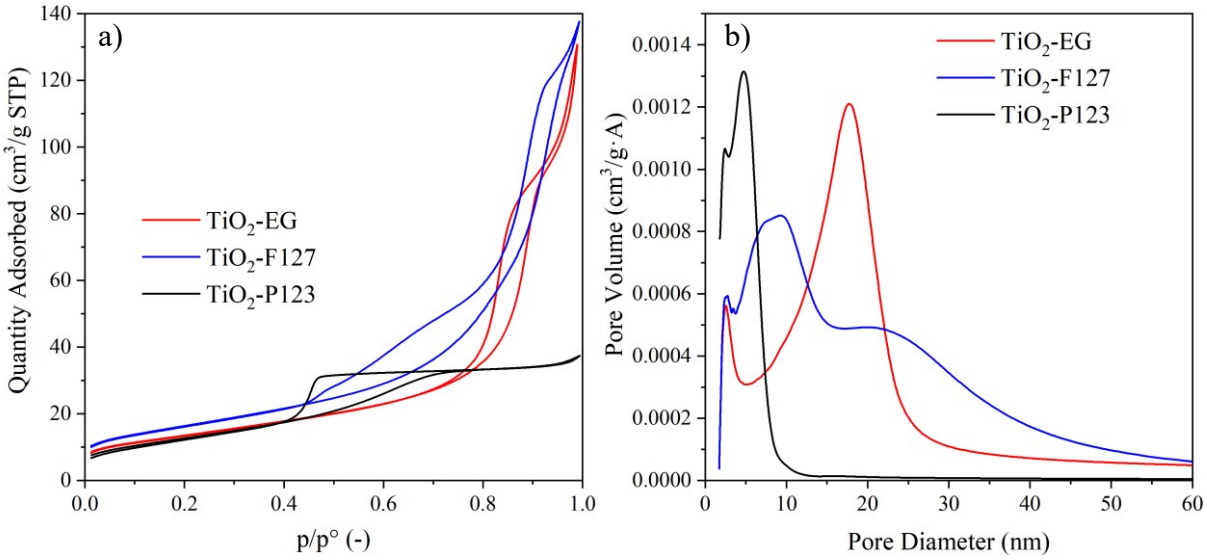

Figure 2: Adsorption-desorption isotherms (a) and pore diameter distribution from the adsorption isotherm (b) of prepared TiO_2 samples.

Table 1: Phase compositions, BET surface area and pore volume of prepared TiO_2 samples.

Sample	Phase composition			BET surface area (m^2/g)	pore V (2r < 21 nm) (cm^3/g)
	Anatase (%)	Rutile (%)	Brookite (%)		
TiO_2-EG	92	1.5	6.5	48	0.13
TiO_2-F127	83.5	16.5	-	58	0.12
TiO_2-P123	100	-	-	82	0.11

The optical properties of the prepared TiO_2 samples were studied using UV-Vis diffuse reflectance spectroscopy (Fig. S2). Reflectance measurements were transformed to Tauc plots (Fig. 3), which were used to determine the band gap energies. The band gap energies were subtracted from the plots using the method described by Makula et al. [26]. TiO_2-EG and TiO_2-F127 exhibited band gap energies of 3.06 and 3.00 eV, respectively, which are closer to the literature data for rutile (3.0 eV) than for anatase (3.2 eV). In contrast, TiO_2-P123 has a

band gap energy of 3.15 eV, which is very close to the literature anatase band gap energy. This could be a result of a composition consisting only of the anatase crystalline phase.

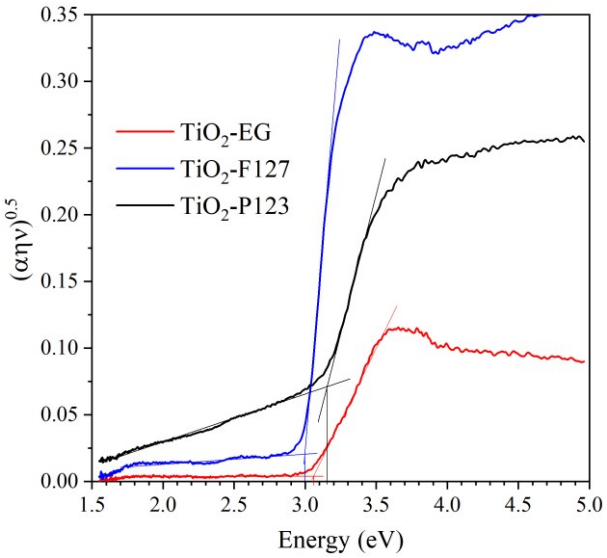

Figure 3: Tauc plots along with subtracted band gap energies of the investigated TiO_2 photocatalysts.

2.2. Results of photocatalytic activity

The evaluation of the influence of various chemicals used for the preparation was conducted for the photocatalytic reduction of carbon dioxide. The main products from the photocatalytic reduction of CO_2 are methane and carbon monoxide, however, hydrogen is also produced. Hydrogen is formed from the water splitting side reaction and is a competitive reaction to CO_2 reduction. It is important to mention that the water oxidation is essential for CO_2 reduction. Water molecules are oxidized by holes to form H^+ ions (1-2), which then react with CO_2 molecules and electrons to produce carbonaceous products. What kind of product is formed is dependent on the number of H^+ ions and electrons participating in the reaction (3-6). H^+ ions can also be reduced by electrons to form hydrogen (7), however, as mentioned above, this is a competitive reaction since it consumes reactants (H^+ and e^-) needed for CO_2 reduction. The yields of individual products obtained from the photocatalytic reduction of CO_2 as a function of time are depicted in Figure 4.

$$2H_2O + 4h^+ \rightarrow O_2 + 4H^+ \quad (1)$$

$$H_2O + h^+ \rightarrow \cdot OH + H^+ \quad (2)$$

$$CO_2 + 2H^+ + 2e^- \rightarrow CO + H_2O \quad (3)$$

$$CO_2 + 4H^+ + 4e^- \rightarrow HCHO + H_2O \quad (4)$$

$$CO_2 + 6H^+ + 6e^- \rightarrow CH_3OH + H_2O \quad (5)$$

$$CO_2 + 8H^+ + 8e^- \rightarrow CH_4 + 2H_2O \quad (6)$$

$$2H^+ + 2e^- \rightarrow H_2 \quad (7)$$

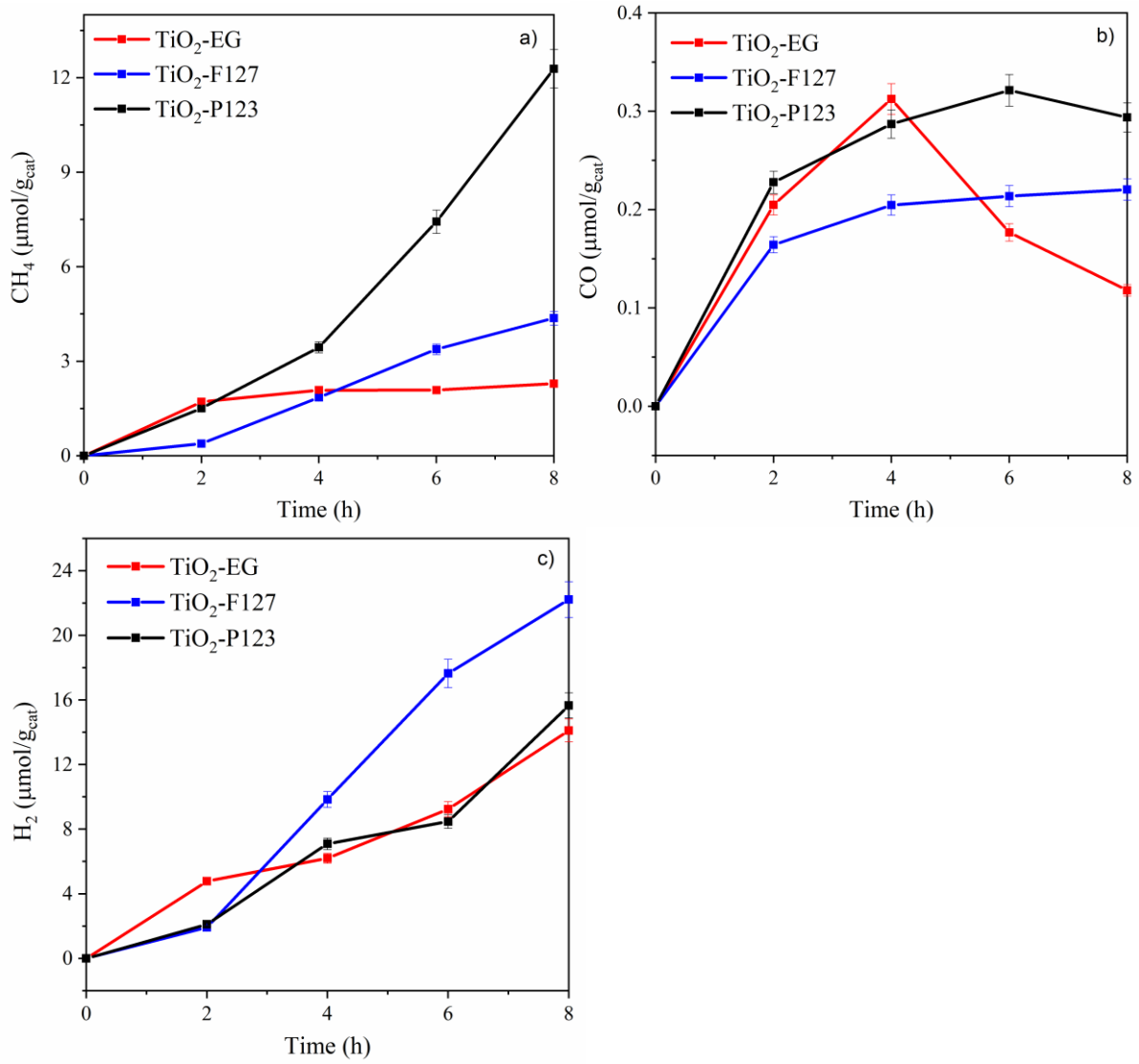

Figure 4: Yields of methane (a), carbon monoxide (b) and hydrogen (c) obtained from the photocatalytic reduction of carbon dioxide at pH=12 in the presence of prepared photocatalysts.

For the sake of easier comparison of the photocatalytic activity, product yields after 8 hours were compared in the presence of each photocatalyst (Fig. 5). Since the photocatalytic reduction of carbon dioxide lacks any kind of standardization, reference experiments were

conducted in the presence of TiO_2 P25 (Evonik). P25 is often considered as a benchmark material in photocatalysis.

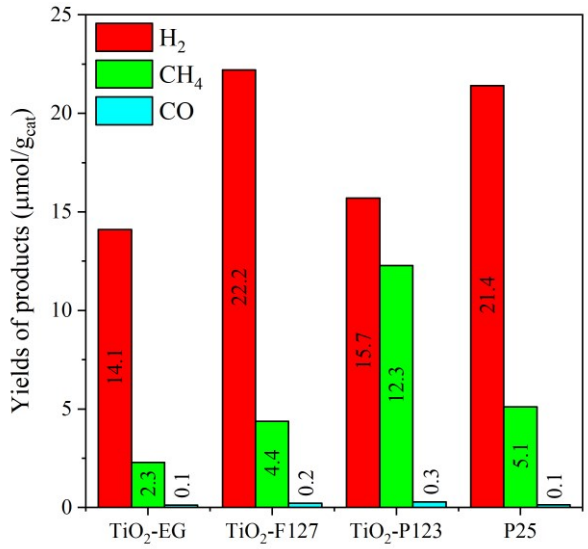

Figure 5: Comparison of products' yields in the presence of prepared photocatalysts and P25.

The efficiency of a photocatalyst can also be quantified by its quantum efficiency. Quantum yield, in the context of semiconductors, represents the number of times a reaction takes place per photon absorbed by the system during any radiation-induced process. One of the crucial factors necessary for computing the quantum yield is accurately determining the quantity of absorbed photons. Nevertheless, ascertaining this figure can be a formidable undertaking due to the pervasive presence of light scattering and reflection caused by suspended photocatalyst particles. To tackle this challenge, an estimation of the absorbed photon count is derived from the incident light intensity, denoted as I_0. Incident light intensity signifies the quantity of photons with a specific wavelength that impinge upon the photoreactor window. This leads to the definition of the apparent quantum yield [27]. Apparent quantum yields were computed for each photocatalyst, and the outcomes, along with the calculations, are presented in the Supplementary materials. The apparent quantum yield of the most active photocatalyst (TiO_2-P123) reached 1.38 %, almost twice as high as that of the TiO_2-EG photocatalyst (see Supplementary materials).

The differences in reactants and synthesis parameters led to different phase compositions (Table 1) and structural properties of TiO_2. The morphology was investigated using a field emission scanning electron microscope (FE-SEM) (Fig. 6). Distinct differences in morphology are clearly visible. The TiO_2-EG image shows microspheres with diameter of 300-400 nm, composed of many < 50 nm sized particles. In contrast, much larger (above 1

μm) structures were observed for TiO_2-F127 and TiO_2-P123, both of which are composed of < 50 nm sized nanoparticles.

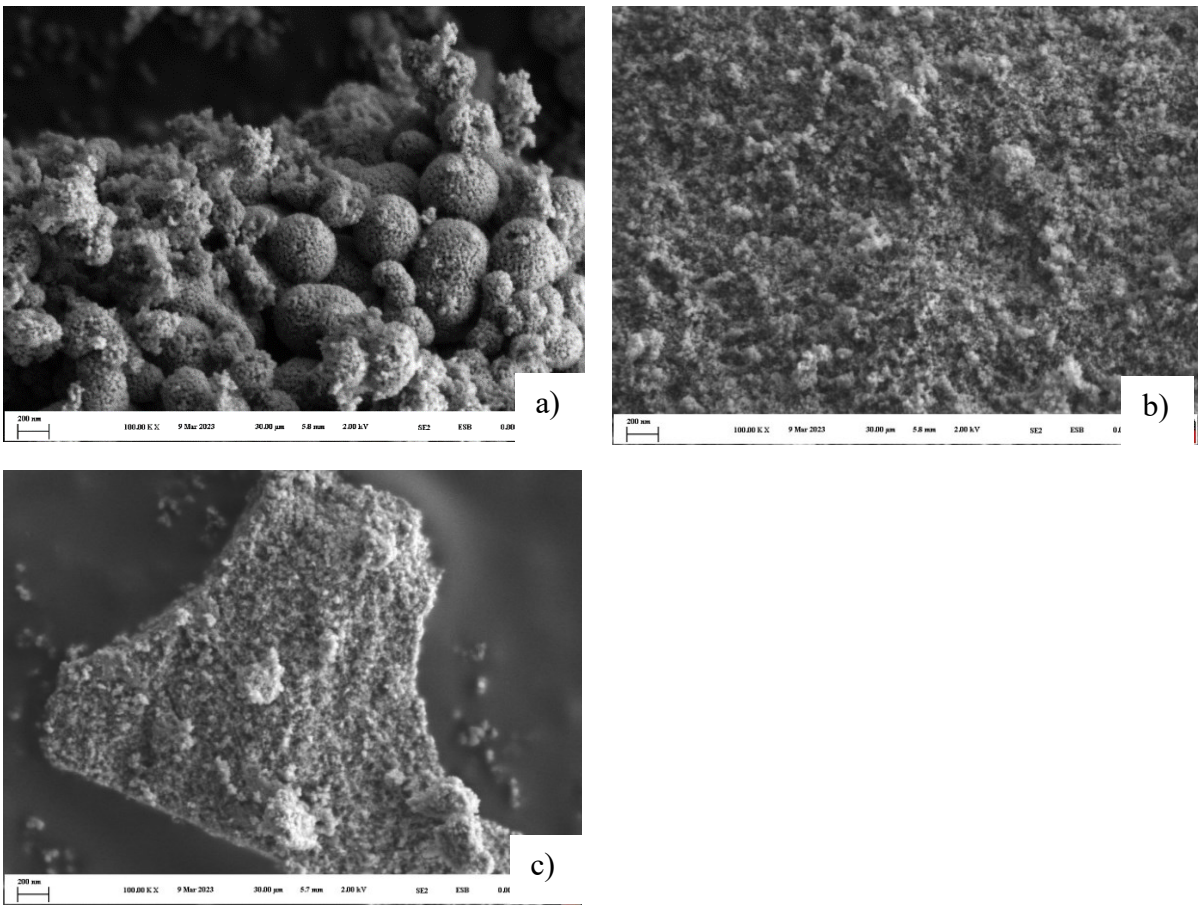

Figure 6: FE-SEM images of TiO_2-EG (a), TiO_2-F127 (b) and TiO_2-P123 (c) with 100.000 x magnification.

Despite the differences in morphology, the specific surface area is the lowest for TiO_2-EG, slightly higher for TiO_2-P123 and even higher for TiO_2-F127 (Table 1). Since photocatalysis occurs on the surface of the photocatalyst, the surface characterization was conducted using XPS analysis (Fig. 7). Nevertheless, the atomic concentration of individual components on the surface of all prepared materials was the same, within the margin of error (Table 2).

Table 2: Atomic component surface concentration based on XPS analysis.

Sample	Ti 2p (IV) (at.%)	Ti 2p (III) (at.%)	O 1s A (at.%)	O 1s B (at.%)	O 1s C (at.%)
TiO_2-EG	98.21	1.79	86.35	8.14	5.51
TiO_2-F127	98.07	1.93	85.8	8.45	5.75

TiO_2-P123	98.08	1.92	84.87	9.15	5.98

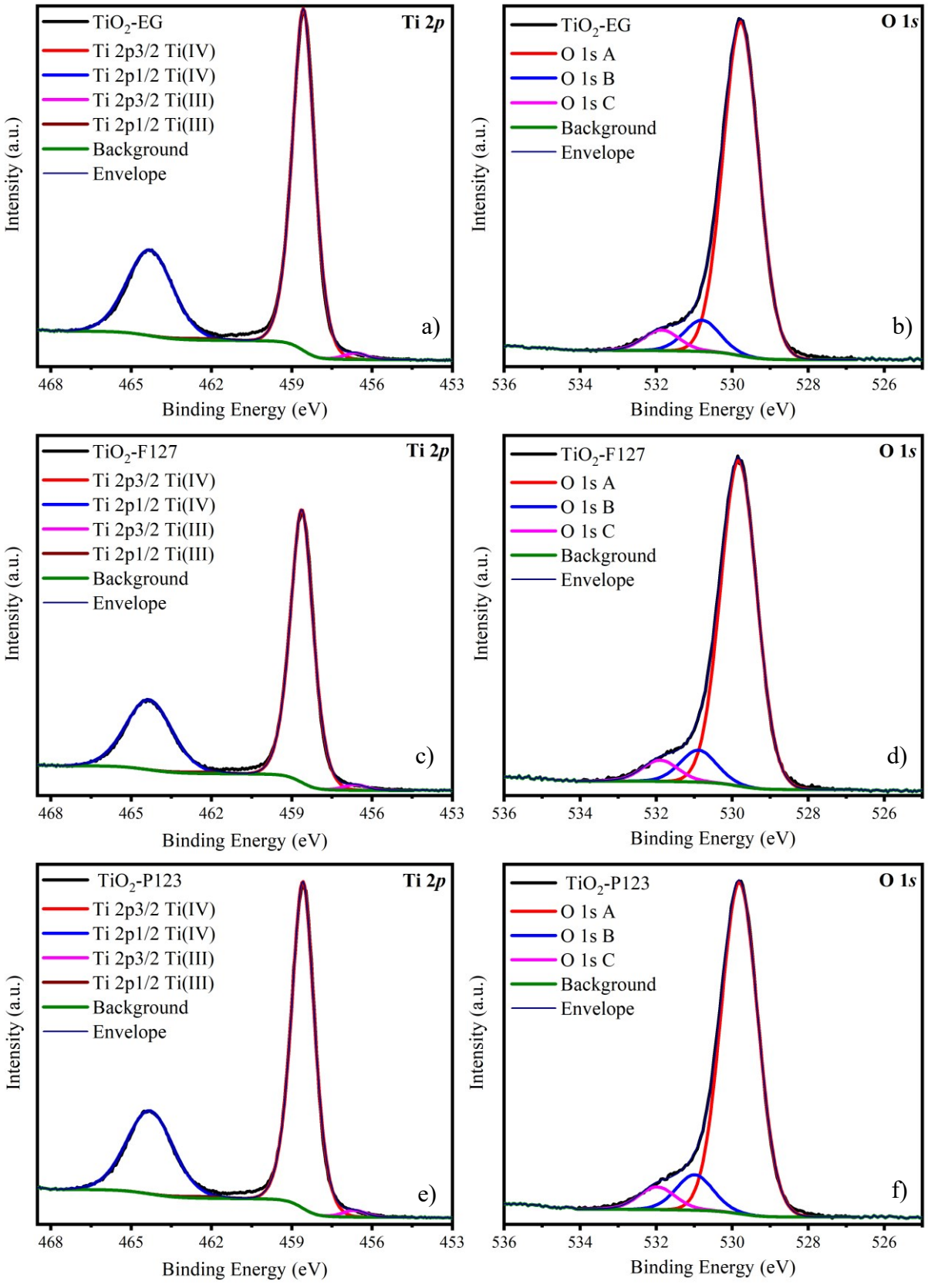

Figure 7: XPS Ti 2p and O 1s spectra of TiO_2-EG (a,b), TiO_2-F127 (c,d) and TiO_2-P123 (e,f).

Regarding the highest photocatalytic activity, one might say the most active of the prepared TiO_2 samples was TiO_2-F127. It exhibited the highest hydrogen production, most likely connected to the presence of a heterojunction between anatase and rutile phases. However, to assess the CO_2 reduction efficiency, it is essential to evaluate the yields of methane and carbon monoxide, as hydrogen is not a product of the photocatalytic reduction of CO_2.

The photocatalytic reduction of CO_2 to CH_4 and CO competes with the photocatalytic water splitting to H_2. Consequently, the selectivity for CO_2 photocatalytic reduction was assessed using Equation (8) [4].

$$\text{Selectivity to } CO_2 \text{ reduction } (\%) = \frac{[2r(CO) + 8r(CH_4)]}{[2r(CO) + 8r(CH_4) + 2r(H_2)]} \cdot 100\% \quad (8)$$

The proportions of CH_4 and CO yields, as well as the selectivity for CO_2 photocatalytic reduction (after 8 hours of irradiation) in the presence of the investigated photocatalysts, are compared in Fig. 8.

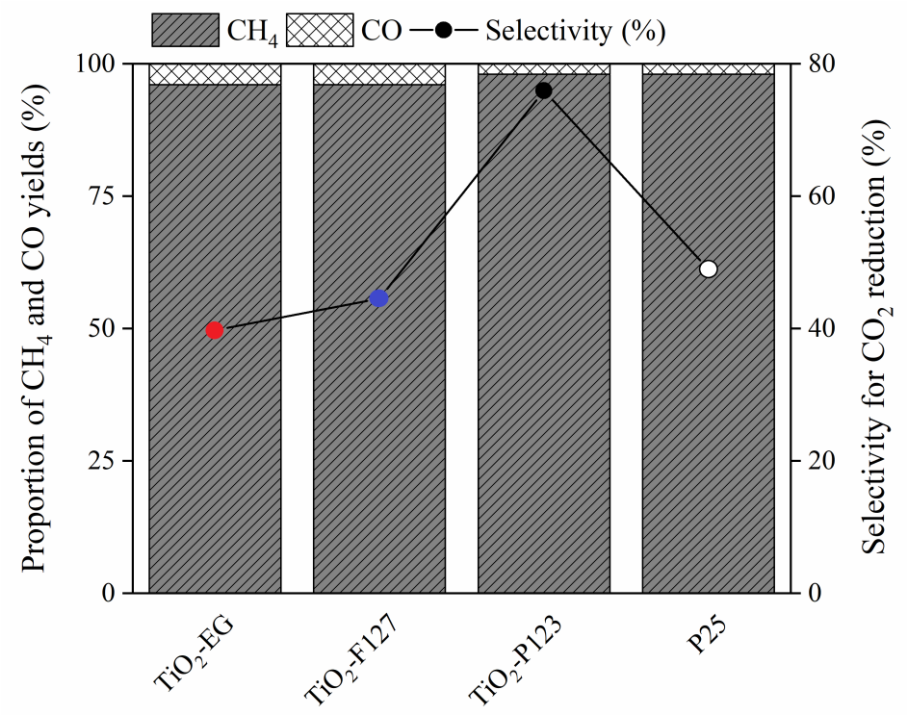

Figure 8: Proportion of CH_4, CO and H_2 yields (after 8 hours of irradiation) and selectivity to the CO_2 photocatalytic reduction.

Figure 8 illustrates that TiO_2-P123 exhibited the highest selectivity for the photocatalytic reduction of CO_2. In contrast, for the photocatalysts P25 and TiO_2-F127, the majority of generated electrons are utilized for hydrogen production, as indicated by Eq. 7, resulting in a relatively low selectivity for CO_2.

It is quite surprising the highest yields of methane were obtained in the presence of the TiO_2-P123 photocatalyst, which consists of pure anatase. These methane yields were more than twice as high as those observed with P25. The reason behind the superior photocatalytic activity of pure anatase may lie in its electronic structure. To investigate this further, photoelectrochemical measurements were conducted. Photocurrent generation was measured in two settings. The first setting was measured across various wavelengths with a step of 10 nm and external potentials with a step of 100 mV. In this case, the sample was irradiated for 5 s and kept in the dark for 5 s before changing the wavelength (Fig. 9a). The presented results were recorded at an external potential of 1 V, which significantly reduces the recombination of charge carriers and essentially provides information about the quantity of generated charge carriers. More generated charge carriers do not necessarily mean higher photocatalytic activity, it is clear samples TiO_2-EG and TiO_2-F127 either have significantly higher recombination rate of charge carriers than TiO_2-P123 or the electrons transfer to lower potential level of rutile conduction band due to type II heterojunction and no longer possesses the reduction power to reduce CO_2 molecule to CH_4. The samples TiO_2-EG and TiO_2-F127 exhibited significantly higher generating of photocurrent. The photocurrent did not even reach baseline when the light was shut off, suggesting that 5 s was not long enough for the electrons and holes to completely recombine. We also investigated the stability of produced charge carriers over time by prolonging the open and close time of the shutter. The measurement was conducted at a single wavelength of 350 nm (Fig. 9b). The results show a trend of decreased photocurrent over time, with the highest decrease recorded for the TiO_2-EG sample.

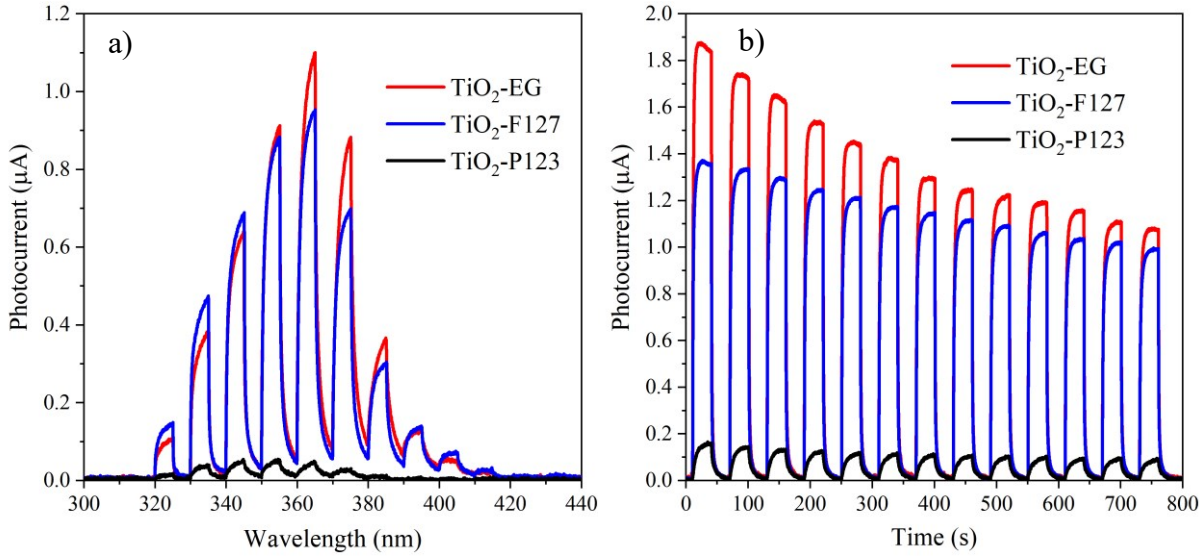

Figure 9: Photocurrent generation at different wavelengths and applied potential 1 V with 5 s open/close shutter (a) and applied potential 1 V and wavelength 350 nm with 30 s open/close shutter (b).

The explanation for the lower photocatalytic activity toward CO_2 reduction of samples consisted of multiple phases is based on two key factors. While it is widely accepted that heterojunctions are beneficial in photocatalysis due to their ability to significantly lower the recombination rate of charge carriers, in the case of heterojunction type II which formed between anatase and rutile, electrons lose reduction power, and holes lose oxidation power. It is not entirely clear whether anatase or rutile has the higher reduction potential, meaning a more negative conduction band potential. Jankulovska et al. experimentally determined that anatase possesses the higher reduction potential [28]. However, more recent studies claim the opposite, suggesting that rutile has to more negative conduction band potential [29, 30]. The band alignment of anatase and rutile is influenced by various factors, including the preparation method and pH of the reaction conditions. In any case, the connection between anatase and rutile leads to a heterojunction type II, which, in turn, results in a decrease in reduction power as electrons migrate from the more negative conduction band to the conduction band with a more positive potential, and a decrease in oxidation power as holes migrate from the more positive valence band to the more negative valence band.

In addition, it has been confirmed that rutile is more prone to oxygen adsorption at its surface [29] and its subsequent reduction to superoxide ions (9). However, both this reactions and hydrogen formation are not desirable in the context of the photocatalytic reduction of carbon

dioxide. Both of these reactions consume electrons that can no longer be used for the reduction of CO_2 to CH_4.

$$O_2 + e^- \rightarrow \cdot O_2^- \qquad (9)$$

Based on literature reviews, the efficiency of photocatalytic processes can be influenced by various factors, such as specific surface area, porosity, band gap energy, percentage of doping elements, and crystallite size. Figure 10 illustrates the correlation between textural properties (specific surface area) and the combined yields of CH_4 and CO.

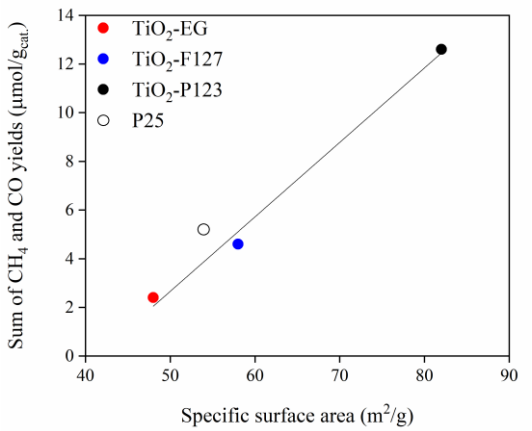

Fig. 10. Correlation between the product yields of photocatalytic CO_2 reduction and specific surface area in presence of investigated photocatalysts and P25.

The ability of TiO_2 to adsorb CO_2 molecules is a critical factor in determining its photocatalytic CO_2 reduction activity. Increasing the specific surface area, and thus the number of surface active sites, benefits the CO_2 adsorption capacity of TiO_2 [31, 32]. The increased specific surface area provides more exposed active sites for reactant molecules (CO_2 and H_2O) to adsorb and subsequently undergo photocatalytic reactions. As a result, the probability of reactant molecules coming into contact with the photocatalyst's active sites increases, leading to enhanced reaction rates. A higher specific surface area also results in a greater number of active sites available for light absorption [32]. Consequently, a larger fraction of incident photons can be absorbed by the photocatalyst, leading to the increased generation of electron-hole pairs and initiating photocatalytic reactions. In photocatalysis, the efficiency of charge separation and transfer plays a crucial role in achieving high photocatalytic activity. A larger specific surface area facilitates shorter electron transfer

pathways, reducing charge recombination losses. This, in turn, improves charge separation and the utilization of photoinduced electrons and holes for redox reactions [33]. The data presented in Fig. 10 confirms that the production of CH_4 and CO increases with an increasing specific surface area which is in alignment with the above statements.

Based on the above findings, it can be inferred that the process of synthesizing mesoporous TiO_2 (via the template-free route and the template-based route using two different copolymers of poly(ethylene oxide) and poly(propylene oxide)) leads to the creation of photocatalysts with distinct phase compositions and significantly impact the specific surface area. Importantly, these two factors play a crucial role in influencing the photocatalytic reduction of CO_2, consequently affecting the yields of methane and carbon monoxide.

3. Conclusions

In summary, our investigation of various synthesis procedures using poly(ethylene oxide) and poly(propylene oxide) copolymers has revealed the significant impact of chemical choice on the yield of photocatalytic CO_2 reduction. This improvement is primarily attributed to variations in phase structure and specific surface area. The pure anatase form (TiO_2-P123) exhibited the highest efficiency and selectivity for CO_2 reduction, while photocatalysts containing both rutile and anatase (TiO_2-EG, TiO_2-F127, and P25) displayed lower photoactivity. This reduction in efficiency was due to the formation of a type II heterojunction between anatase and rutile, leading to reduced reducing power, and rutile's higher affinity for oxygen adsorption, resulting in diminished photoactivity through the generation of superoxide ions. Furthermore, the most active photocatalyst, TiO_2-P123, possessed the highest specific surface area, providing more reactive sites, thereby enhancing light absorption efficiency and extending the lifetime of photogenerated electron-hole pairs. This improvement in photocatalytic activity was confirmed by calculated apparent quantum yields. In conclusion, our study underscores the potential for enhancing CO_2 photocatalytic reduction by employing a systematic and rational synthesis approach with mesoporous TiO_2 photocatalysts.

Acknowledgement

The work was supported by Large Research Infrastructure ENREGAT (project No. LM2023056), GA CR 21-24268K. The authors also thank the financial support provided by the Slovenian Research and Innovation Agency (Grant Nos. N2-0188, P2-0273 and P1-0134).

Authors contributions

R. M. – investigation, writing – original draft; N. P. – investigation, methodology; F. E. M. – investigation, writing – original draft; R. R. – formal analysis; S. Š. A. – investigation; L. Š. U. – supervision; K. K. – supervision, writing – original draft.

References:

[1] L. Zhao, B.P. Harvey, T. Higuchi, S. Agostini, K. Tanaka, N. Murakami-Sugihara, H. Morgan, P. Baker, J.M. Hall-Spencer, K. Shirai, Ocean acidification stunts molluscan growth at CO_2 seeps, Sci. Total Environ., 873 (2023) 162293.
[2] W.B. Group, Publication: State and Trends of Carbon Pricing 2019, 2019.
[3] R.B. Domínguez-Espíndola, D.M. Arias, C. Rodríguez-González, P.J. Sebastian, A critical review on advances in TiO_2-based photocatalytic systems for CO_2 reduction, Appl. Therm. Eng., 216 (2022) 119009.
[4] M. Filip Edelmannová, M. Reli, P. Nadrah, N. Rozman, R. Ricka, A. Sever Škapin, M. Nosan, U. Lavrenčič Štangar, K. Kočí, A comparative study of TiO_2 preparation method on their photocatalytic activity for CO_2 reduction, Catalysis Today, 413-415 (2023) 113944.
[5] Z. Zhao, Z. Wang, J. Zhang, C. Shao, K. Dai, K. Fan, C. Liang, Interfacial Chemical Bond and Oxygen Vacancy-Enhanced In_2O_3/CdSe-DETA S-scheme Heterojunction for Photocatalytic CO_2 Conversion, Advanced Functional Materials, 33 (2023) 2214470.
[6] J. Wang, Z. Wang, J. Zhang, S.-P. Chai, K. Dai, J. Low, Surface-active site modulation of the S-scheme heterojunction toward exceptional photocatalytic performance, Nanoscale, 14 (2022) 18087-18093.
[7] X. Ke, J. Zhang, K. Dai, K. Fan, C. Liang, Integrated S-Scheme Heterojunction of Amine-Functionalized 1D CdSe Nanorods Anchoring on Ultrathin 2D $SnNb_2O_6$ Nanosheets for Robust Solar-Driven CO_2 Conversion, Solar RRL, 5 (2021) 2000805.

[8] Z. Zhao, L. Duan, Y. Zhao, L. Wang, J. Zhang, F. Bu, Z. Sun, T. Zhang, M. Liu, H. Chen, Y. Yang, K. Lan, Z. Lv, L. Zu, P. Zhang, R. Che, Y. Tang, D. Chao, W. Li, D. Zhao, Constructing Unique Mesoporous Carbon Superstructures via Monomicelle Interface Confined Assembly, Journal of the American Chemical Society, 144 (2022) 11767-11777.
[9] K. Lan, Y. Xia, R. Wang, Z. Zhao, W. Zhang, X. Zhang, A. Elzatahry, D. Zhao, Confined Interfacial Monomicelle Assembly for Precisely Controlled Coating of Single-Layered Titania Mesopores, Matter, 1 (2019) 527-538.
[10] K. Lan, R. Wang, W. Zhang, Z. Zhao, A. Elzatahry, X. Zhang, Y. Liu, D. Al-Dhayan, Y. Xia, D. Zhao, Mesoporous TiO_2 Microspheres with Precisely Controlled Crystallites and Architectures, Chem, 4 (2018) 2436-2450.
[11] Z. Zhao, Y. Zhao, R. Lin, Y. Ma, L. Wang, L. Liu, K. Lan, J. Zhang, H. Chen, M. Liu, F. Bu, P. Zhang, L. Peng, X. Zhang, Y. Liu, C.-T. Hung, A. Dong, W. Li, D. Zhao, Modular super-assembly of hierarchical superstructures from monomicelle building blocks, Science Advances, 8 eabo0283.
[12] H. Yang, K. Dai, J. Zhang, G. Dawson, Inorganic-organic hybrid photocatalysts: Syntheses, mechanisms, and applications, Chinese Journal of Catalysis, 43 (2022) 2111-2140.
[13] L. Liu, Z. Wang, J. Zhang, O. Ruzimuradov, K. Dai, J. Low, Tunable Interfacial Charge Transfer in a 2D–2D Composite for Efficient Visible-Light-Driven CO_2 Conversion, Advanced Materials, 35 (2023) 2300643.
[14] X. Li, J. Zhang, Y. Huo, K. Dai, S. Li, S. Chen, Two-dimensional sulfur- and chlorine-codoped g-C_3N_4/CdSe-amine heterostructures nanocomposite with effective interfacial charge transfer and mechanism insight, Applied Catalysis B: Environmental, 280 (2021) 119452.
[15] L.-S. Zhong, J.-S. Hu, L.-J. Wan, W.-G. Song, Facile synthesis of nanoporous anatase spheres and their environmental applications, Chem. Commun. (Cambridge, U. K.), (2008) 1184-1186.
[16] T. Zhang, J. Low, K. Koh, J. Yu, T. Asefa, Mesoporous TiO_2 Comprising Small, Highly Crystalline Nanoparticles for Efficient CO_2 Reduction by H_2O, ACS Sustainable Chemistry & Engineering, 6 (2018) 531-540.
[17] X. Ma, K. Hao, Y. Dai, L. Song, Q. Yu, X. Yin, Z. Wang, Enhanced Visible-Light Photocatalytic Activity by the Comprehensive Effects of Mesoporous and N-Doping at the Meso-N-TiO_2 Nanocatalysts, ChemistrySelect, 6 (2021) 6029-6036.
[18] X.-M. Chen, Z.-J. Liu, J.-T. Tang, C.-L. Teng, T.-J. Cai, Q. Deng, La-modified mesoporous TiO_2 nanoparticles with enhanced photocatalytic activity for elimination of VOCs, Journal of Porous Materials, 22 (2015) 361-367.

[19] T. Hu, K. Dai, J. Zhang, S. Chen, Noble-metal-free Ni_2P modified step-scheme $SnNb_2O_6$/CdS-diethylenetriamine for photocatalytic hydrogen production under broadband light irradiation, Applied Catalysis B: Environmental, 269 (2020) 118844.
[20] Z. Zhao, X. Li, K. Dai, J. Zhang, G. Dawson, In-situ fabrication of Bi_2S_3/$BiVO_4$/$Mn_{0.5}Cd_{0.5}S$-DETA ternary S-scheme heterostructure with effective interface charge separation and CO_2 reduction performance, Journal of Materials Science & Technology, 117 (2022) 109-119.
[21] J. Wang, Z. Wang, K. Dai, J. Zhang, Review on inorganic–organic S-scheme photocatalysts, Journal of Materials Science & Technology, 165 (2023) 187-218.
[22] J.I. Langford, A.J.C. Wilson, Scherrer after sixty years: A survey and some new results in the determination of crystallite size, J. Appl. Crystallogr., 11 (1978) 102-113.
[23] E.P. Meagher, G.A. Lager, Polyhedral thermal expansion in the TiO_2 polymorphs; refinement of the crystal structures of rutile and brookite at high temperature, Can. Mineral., 17 (1979) 77-85.
[24] O. Carp, C.L. Huisman, A. Reller, Photoinduced reactivity of titanium dioxide, Prog. Solid State Chem., 32 (2004) 33-177.
[25] M. Thommes, K. Kaneko, A.V. Neimark, J.P. Olivier, F. Rodriguez-Reinoso, J. Rouquerol, K.S.W. Sing, Physisorption of gases, with special reference to the evaluation of surface area and pore size distribution (IUPAC Technical Report), Pure Appl. Chem., 87 (2015) 1051-1069.
[26] P. Makuła, M. Pacia, W. Macyk, How To Correctly Determine the Band Gap Energy of Modified Semiconductor Photocatalysts Based on UV–Vis Spectra, J. Phys. Chem. Lett, 9 (2018) 6814-6817.
[27] R. Ricka, M. Přibyl, K. Kočí, Apparent quantum yield – Key role of spatial distribution of irradiation, Applied Catalysis A: General, 658 (2023) 119166.
[28] M. Jankulovska, T. Berger, T. Lana-Villarreal, R. Gómez, A comparison of quantum-sized anatase and rutile nanowire thin films: Devising differences in the electronic structure from photoelectrochemical measurements, Electrochim. Acta, 62 (2012) 172-180.
[29] M. Buchalska, M. Kobielusz, A. Matuszek, M. Pacia, S. Wojtyła, W. Macyk, On Oxygen Activation at Rutile- and Anatase-TiO_2, ACS Catal., 5 (2015) 7424-7431.
[30] D.O. Scanlon, C.W. Dunnill, J. Buckeridge, S.A. Shevlin, A.J. Logsdail, S.M. Woodley, C.R.A. Catlow, M.J. Powell, R.G. Palgrave, I.P. Parkin, G.W. Watson, T.W. Keal, P. Sherwood, A. Walsh, A.A. Sokol, Band alignment of rutile and anatase TiO_2, Nat Mater, 12 (2013) 798-801.

[31] J. Low, B. Cheng, J. Yu, Surface modification and enhanced photocatalytic CO_2 reduction performance of TiO_2: a review, Appl. Surf. Sci., 392 (2017) 658-686.
[32] X. Long, X. Wei, Y. Qiu, Y. Song, L. Bi, P. Tang, X. Yan, S. Wang, J. Liao, TiO_2 aerogel composite high-efficiency photocatalysts for environmental treatment and hydrogen energy production, Nanotechnol. Rev., 12 (2023).
[33] F. Zhang, X. Wang, H. Liu, C. Liu, Y. Wan, Y. Long, Z. Cai, Recent Advances and Applications of Semiconductor Photocatalytic Technology, Appl. Sci., 9 (2019) 2489.